16 State House Station
Augusta, Maine 04333

MaineDOT

Transportation Research Division

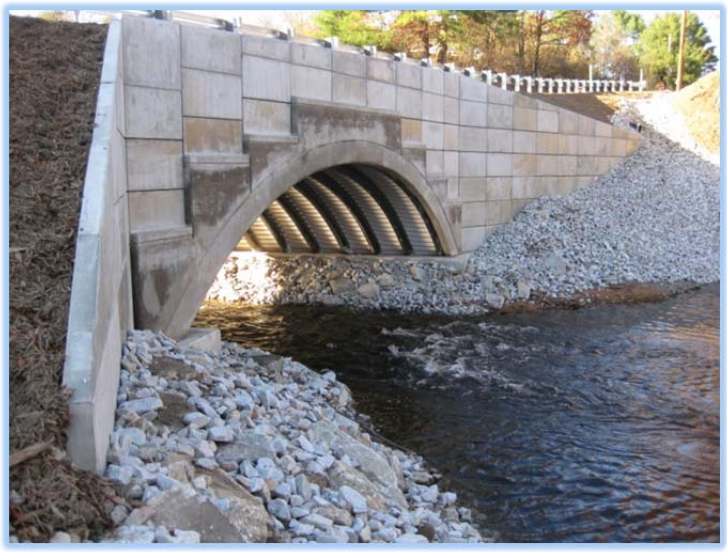

Technical Report 16-02

Bridge-in-a-Backpack™

Task 3.1: Investigate Soil-Structure Interaction – Experimental Design

Final Report – January 2016

Technical Report Documentation Page

1. Report No. ME 16-02	2.	3. Recipient's Accession No.	
4. Title and Subtitle Bridge-in-a-Backpack™ Task 3.1: Investigating Soil – Structure Interaction – Experimental Design		5. Report Date July 2015 6.	
7. Author(s) Harold J. Walton, Ph.D. Candidate Bill Davids, Ph.D., P.E. Melissa Maynard, Ph.D Keenan Goslin, P.E.		8. Performing Organization Report No.	
9. Performing Organization Name and Address University of Maine – Advanced Structures and Composites Center		10. Project/Task/Work Unit No. Project 17891.00 – Task 3.1 11. Contract © or Grant (G) No. Contract # 20111223*2878	
12. Sponsoring Organization Name and Address Maine Department of Transportation		13. Type of Report and Period Covered 14. Sponsoring Agency Code	
15. Supplementary Notes			

16. Abstract (Limit 200 words)

This report includes fulfillment of Task 3.1 of a multi-task contract to further enhance concrete filled FRP tubes, or the Bridge in a Backpack. Task 3 is an investigation of soil-structure interaction for the FRP tubes. Task 3.1 is the design of the experimental system with descriptions of analysis and scaling options for several parameters including arches, decking and load.

The goal of this project is to improve the design efficiency of the buried concrete filled arch bridge system comprised of concrete-filled fiber reinforced polymer (FRP) tube (CFFT) arches through a detailed experimental and computational assessment of soil-structure interaction. Previous research (Bannon 2009; Dagher et al 2012) has assessed the load capacity of an isolated arch; this capacity depends on the tensile strength properties of the composite shell. For a given load or set of loads on the arch the behavior of an isolated arch is documented and predictable, but the soil cover and decking have a large influence on load distribution. Soil both dissipates patch loads from truck tires, spreading the load over a greater area of the arch, and restrains the arch from moving under load; both actions reduce the moment carried by the arch from a truck tire patch or point load. A better understanding of the interaction between the cover soil and the supporting structure is necessary to improve prediction of the loads on the arch and foundation. This project seeks to improve this understanding computationally and experimentally through the testing of subscale buried arch structures. Mimicking the soil-structure interaction response of full-scale structures in these laboratory tests is critical, and is the focus of this report.

17. Document Analysis/Descriptors Arch bridges, concrete filled FRP tubes, soil-structure interaction, Bridge-in-a-Backpack		18. Availability Statement	
19. Security Class (this report)	20. Security Class (this page)	21. No. of Pages 41	22. Price

Project 1023: Research and Development to Advance Buried Composite Bridge Technologies

Task C (Deliverable 1): Scaling of Laboratory Test Bridges

7/8/2015
Harold J. Walton, Ph.D. Candidate
Bill Davids, Ph.D., P.E., John C. Bridge Professor and Chair of Civil and Environmental Engineering
Melissa Maynard, Ph.D., Associate Professor of Civil and Environmental Engineering
Keenan Goslin, P.E., Research Engineer (formerly of Advanced Structures and Composites Center)

University of Maine Advanced Structures and Composites Center and Department of Civil and Environmental Engineering

Table of Contents

Introduction

The goal of this project is to improve the design efficiency of the buried concrete filled arch bridge system comprised of concrete-filled fiber reinforced polymer (FRP) tube (CFFT) arches through a detailed experimental and computational assessment of soil-structure interaction. Previous research (Bannon 2009; Dagher et al 2012) has assessed the load capacity of an isolated arch; this capacity depends on the tensile strength properties of the composite shell. For a given load or set of loads on the arch the behavior of an isolated arch is documented and predictable, but the soil cover and decking have a large influence on load distribution. Soil both dissipates patch loads from truck tires, spreading the load over a greater area of the arch, and restrains the arch from moving under load; both actions reduce the moment carried by the arch from a truck tire patch or point load. A better understanding of the interaction between the cover soil and the supporting structure is necessary to improve prediction of the loads on the arch and foundation. This project seeks to improve this understanding computationally and experimentally through the testing of subscale buried arch structures. Mimicking the soil-structure interaction response of full-scale structures in these laboratory tests is critical, and is the focus of this report.

Arches have been built with a variety of span to depth ratios; typical values range from 5:1 to 3:1. A bridge with a large span to depth ratio will have large footing thrust and small radial displacement compared to a taller arch with the same stiffness. A bridge with a 12 m span and 1.5 m spacing approaches the strength limit for 300 mm diameter arches based on typical truck and soil loading, but this bridge is too large for laboratory testing due to height and cost limitations. A subscale arch with half the height was required to load the arch with an overhead actuator. Figure 1 depicts the planned test setup to be used in the laboratory study, where soil is confined in a self-reacting timber and concrete box and superimposed loads are applied to the soil surface. The self-reacting design was necessary to limit the width of the reaction box and the use of laboratory space given the long duration of the testing period. The box is made self-reacting with through

ties perpendicular to the plane of the arch. Further, one end of the box was a pre-cast concrete reaction wall anchored to the laboratory floor, and the second timber end wall was tied via cables to the pre-cast concrete reaction wall. To minimize the effect of the through ties on arch behavior, ties buried in soil above the arch, the ties were positioned at least 900 mm from the top surface and 150 mm from the bottom surface of the buried structure as shown in Figure 1.

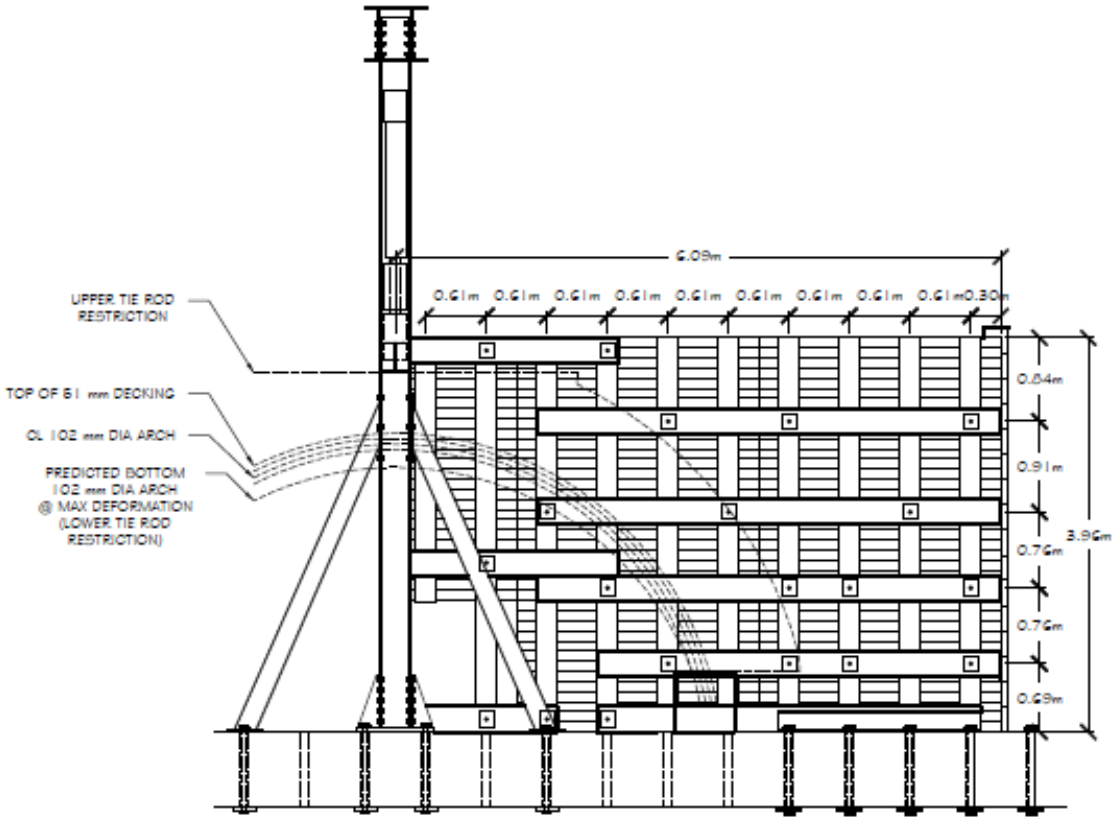

Figure 1. Elevation View of Half of Proposed Test Setup

Overview of Scaling Considerations

To achieve representative soil structure interaction in this test setup, the subscale bridge should have both the same load distribution and horizontal soil pressure as the full-scale bridge. Soil dead load is a major portion of the load on the arch and the distribution of this load must be

preserved; the span and the spacing are scaled with the height of the bridge to maintain volume for a given percent bridge length. Live loads must also be scaled accordingly and are further discussed in the Scaling section. Horizontal soil pressure is dependent on deflection and position from the neutral soil position. There are too many parameters influencing arch stiffness to produce ideal horizontal pressures under all loading conditions, and as a result the lab scale structure was designed based on horizontal pressures caused by the scaled live loading positioned at the apex of the backfilled structure. This is not the only important pressure; alternatively the horizontal pressure profile at the end of backfill or during important truck loading positions could have been selected.

Apex live load is not the critical design live load for most buried bridges because the highest moments produced by apex load are positive beam sign convention moments (tension on bottom) at the apex, which opposes larger negative locked-in backfilling moments. Apex loading is preferable to critical design load locations as a scaling parameter because the moment response is large and the location is well defined; the apex is always in the same location for a given span regardless of rise. Peak positive moment response at the 'shoulder' occurs in varying span locations based on bridge shape, and due to lack of knowledge about load distribution there is less confidence in offset load response. The response to apex load is close to symmetric, differing only by staged backfilling history from side to side on the bridge, and peak vertical pressure should be located directly under the load.

Ultimately, two arch geometries were considered: a short arch with 6.1 m span, 1.2 m rise, 0.76 m spacing, and a tall arch with 6.1 m span, 2.28 m rise, and 0.76 m spacing. The two arch geometries were selected to provide both a high deformation small thrust arch and a low deformation large thrust arch.

CFFT arches have a nonlinear moment curvature relationship; axial compression reduces the crack depth in the concrete making the section stiffer in bending. Concrete does carry some

tensile stress before it is cracked; reloaded concrete will behave differently than uncracked concrete adding complications to the strain-moment relationship. Heavy braided FRP is a difficult material on which to measure strain with foil gauges due to variation in strain behavior between individual fiber tows and the small number of tows measured by a single foil strain gauge. These issues complicate the soil interaction study. Therefore, a steel arch was also developed for soil testing purposes. Steel, prior to yield, is a linear elastic material and the bending stiffness of a steel member is not dependent on axial load or prior loads. Because steel behaves as a uniform homogenous material foil strain gauges are effective at reading bending strain on steel. The steel arch needed to adhere to the same scaling guidelines as the FRP subscale: same load distribution and similar horizontal pressure.

Model Description

All preliminary modeling for this research program is based on the model used for commercial bridge design by Advanced Infrastructure Technologies, with some modifications. The model software was originally developed by Clapp and Davids (2011). This report includes specific modeling decisions for pretest modeling and does not reflect modeling decisions made for analyzing testing results and model verification as specific soil and structural properties were not known while designing the test. Throughout this document beam moment sign convention is assumed unless specifically designated: negative moment causes tension on the top of the arch, positive moment causes compression on the top of the arch.

For the model, displayed conceptually in Figure 2, the arch span is in the global *x*-direction, the arch rise is in the global *y*-direction and the decking between parallel arches is in the global *z*-direction. The model treats a single isolated arch rather than a full bridge. The structural elements in the pretest model are small deformation, 3D Euler-Bernoulli beam elements. Deformations under service level loading peak during backfilling at approximately 50 mm, which is small

compared to the arch span of 12 m for a full scale bridge assumed during analysis, justifying small deformation elements for initial modeling. Euler-Bernoulli beams also do not deform due to shear, which is reasonable because of the large span to depth ratio for an arch and the small beam shear compared to moment or axial load. All loading is assumed symmetric and in-plane; torsion is ignored in this analysis. No loads are applied in the weak axis direction of the arches or the decking.

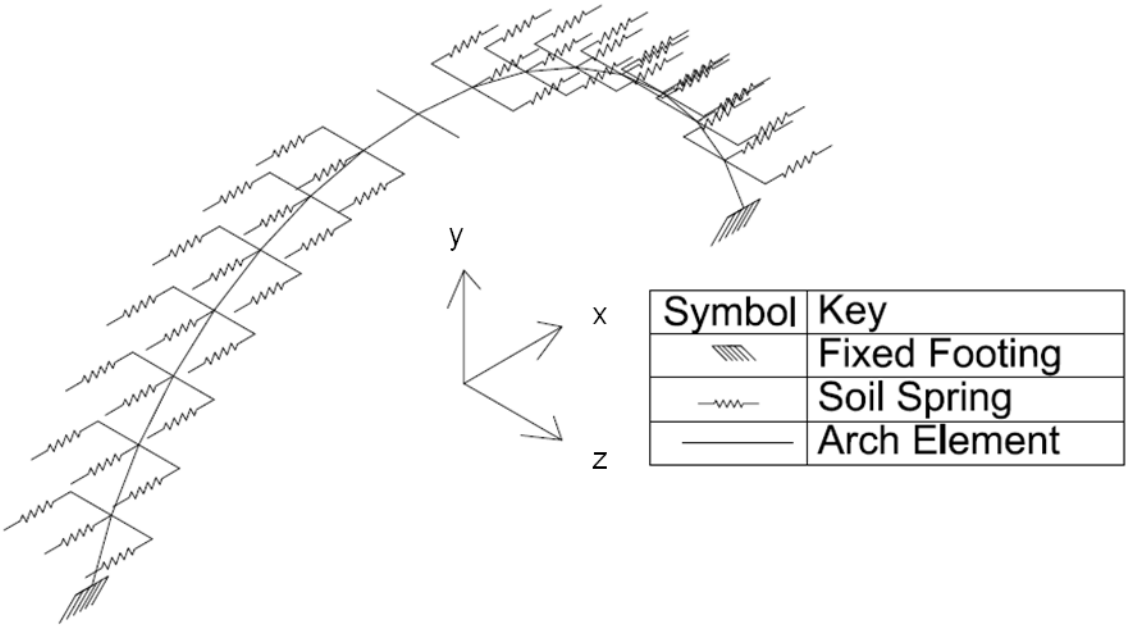

Figure 2. Soil-Spring Model

Arch elements each have equal arc length, and models have 60 elements to represent the full span of the arch, starting at the right hand support of the arch. Euler-Bernoulli beam elements have instant convergence for a straight member, but the curved arch is represented by straight elements – more elements will better represent the arch geometry. Nonlinear soil springs and bending stiffness are used in this model, so a brief convergence study was done to look at the effect of additional nodes, showing that 60 elements gives convergent results. This is consistent

with the level of discretization required to model a nonlinear, free-standing arch (Bannon 2009, Walton 2011).

Decking

Another model discretization option is the addition of beam elements transverse to the plane of the arch representing decking. Transverse decking is modeled as a series of independent rotated beams with an appropriate material and thickness based stiffness in the element local 2-direction (through the decking thickness) and an arbitrarily high torsional stiffness and bending stiffness in the element 3-direction (in the plane of the decking). Decking elements are rigidly connected to the arch nodes, and the ends of the decking sections are fixed against translation in the global *z*-direction and rotation in the global *x*- and *y*-directions. These boundary conditions mimic symmetric response consistent with multiple, parallel arches and uniform soil pressure. While soil pressure is not uniform under live loading or surcharge, this is still a reasonable simplification for a 2D simulation of a 3D system, and more realistic than modeling transverse decking with cantilevers.

The model can have multiple elements per section of decking and the additional decking elements are all connected to soil elements. An infinitely rigid deck will produce the same deflections as the arch and will not affect any results in the model. An infinitely flexible deck will deform away from the soil and will have all active soil pressures, which will decrease backfilling moments (when soil pressure causes moment) and will increase live load pressure (when soil restraint strengthens the arch). Realistic decking produces an effect somewhere between these two cases. Three models were created: zero-deck, two-deck and four-deck, indicative of the number of decking elements per arch node. The zero-deck model produces end of backfill moments 3% lower and apex live moments 1% lower than the two-deck model, which does not justify the additional run time for decking elements. Additional decking elements produce less

effect: a four-deck model was within 0.5% moment and deflection with the two-deck model for all important locations such as footings, shoulders, and apex under all load conditions.

Soil is modeled as a series of nonlinear spring elements connected at each decking node and arch node with horizontal force dependent on the change in spring length (x displacement). The deflection is zeroed from the point where the node of interest was first buried and compacted; the zero position for a spring is not the zero deflection position for the arch. The soil spring modeling approach and the soil spring load-deformation relationship developed from NCHRP Report No. 343 (1991) are given by Clapp and Davids (2011), and discussed in more detail later in this report. Soil was modeled using typical design assumptions: a medium density granular soil (2.0 Mg/m3) with a friction angle (ϕ) of 37° and an at-rest earth pressure coefficient (K_0) 0.45.

Boundary Conditions

For simplicity, the arches are modeled as fixed at the footing for all pretest analyses. During field implementation arches are cast in a large reinforced concrete footing that restrains the arch end rotations and deflections. The concrete mass either acts as a spread footing to distribute the vertical load into the underlying soil, while soil behind the footing prevents horizontal displacements, or the foundation is built on piles, which help transfer the vertical and horizontal arch loads to the soil. In lab testing the arches were cast into a concrete spread footing, but unlike a typical bridge there was no soil under the footings; the footings were supported by the rigid reinforced concrete lab floor.

Horizontal restraint was two opposite extremes to surround the real world conditions: rigidly linked footings and low base friction footings. During initial lab testing, the two footings were connected with steel bars that span the direction of the arch, and inline load cells measured the horizontal thrust between the footings. Implemented throughout backfill and during initial loading, this condition is equivalent to a rock anchored footing or a very rigid soil or pile

foundation where basically no footing movement is allowed. The steel bars were removed after initial testing and additional live loads and the ultimate loads were applied with sliding footings. The untied footings were still fixed against rotation the end of the arch relative to the footing, only now the footing was allowed to move along the span direction with a thin plastic pad under the footing to reduce the base friction. Horizontal restraint was provided by the soil behind the footing. These two tested cases were intended to bound the possible soil to footing interactions of the arch bridge system. One discrepancy between real-world bridges and the experimental test is that the soil does not extend below the concrete floor, so less soil was mobilized by the footings than in an actual bridge, which reduces sliding footing restraint compared to a full scale bridge.

Soil

Currently, the bridges are designed using soil springs that do not account for additional stiffness from compaction and represent the transition from at-rest pressure to passive pressure with a single linear region (Clapp and Davids 2011). Compaction increases the at-rest earth pressure, increasing spring stiffness. Soil passive response is expected to be nonlinear, gaining more stiffness with less deflection near at-rest pressure, before shear banding develops, than when soil pressures are close to fully passive. Vertical surcharge through the soil is based on the Boussinesq distribution for load acting on the surface of the soil (Holtz and Kovacs, 1981). This distribution assumes an elastic homogenous soil mass; the actual soil mass is compacted layers of fill and will tend to form stress layers, causing a lower load directly under the surface load and a greater load away from the surface load, closer to the Westergaard theory. Horizontal soil stress from a surcharge load is the vertical soil stress at a given point multiplied by the current horizontal pressure coefficient.

Soil dead load, the weight of the soil, is assessed using equivalent fluid pressure. The vertical soil stress at any point along the arch is the local soil depth multiplied by the soil density.

Horizontal soil loads are more complicated because they are based on equivalent fluid pressure and the movement of the arches. When an arch moves away from the soil mass the soil is in the active region, decreasing the horizontal stress; when the arch moves toward the soil mass it is in the passive region increasing the horizontal stress. Active and passive regions are based on the NHCRP (1991) curve for medium-dense sands behind a cantilever wall, with the plot shown in Figure 3, normalized with wall height (h); for this analysis the arch height is used as the wall height. Often the soil against the arch is neither fully active nor fully passive, and the soil stress and soil stiffness for a particular node are based on the movement of the node relative to the total arch height and are linearly interpolated from Figure 3. Typical bridge design uses the uncompacted soil curve, which is considered conservative, but is less likely to produce the actual laboratory displacements and stresses. When the displacement is greater than $0.009h$, the soil is fully active with $K = 0.25$, when displacement is less than $-0.016h$ it is fully passive with $K = 4.0$. In between, there is a series of linear portions that approximate the NCHRP curve. Figure 3 compares the compacted and uncompacted soil curves. The horizontal pressure is the total vertical pressure (from live load and from soil loads) multiplied by the horizontal pressure coefficient calculated based on deflection.

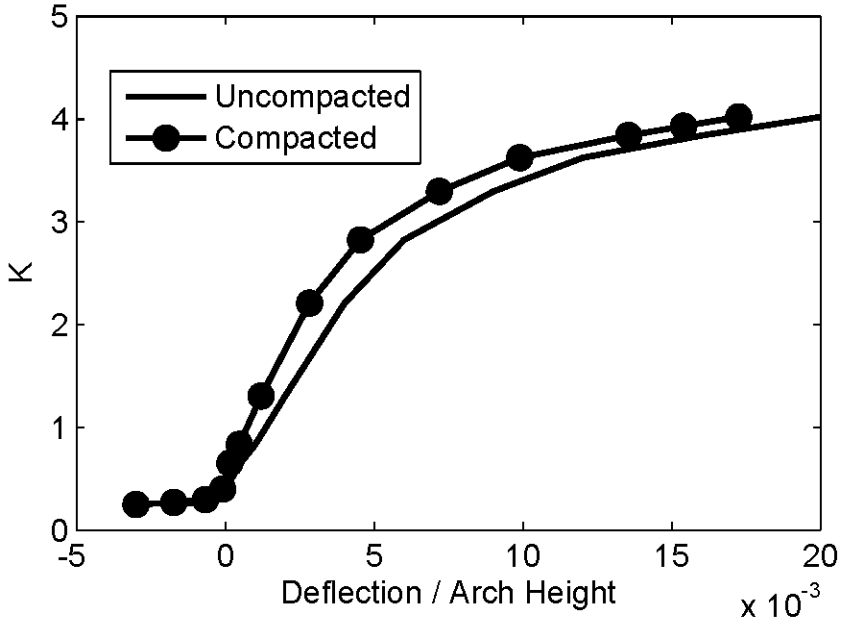

Figure 3. Comparison of Compacted and Uncompacted Soil Stiffness

Compacted and uncompacted soil assumptions produce different model outputs for a given arch. The difference is more pronounced for the taller arch, where the horizontal soil forces are higher because the arch is taller. During backfill, the stiffer compacted soil pushes harder on the arch and causes approximately 10% larger moments at the footing and larger displacements. Radial displacements caused by complete soil backfill are compared for compacted and uncompacted soils assuming a tall, full-scale arch in Figure 4 and assuming a short full-scale arch in Figure 5 with 5.8 m of soil over both footings and 1.22 m of soil over the apex. The change in displacement from a subsequent apex line live load with the design tandem load described in the load section is also shown in Figures 4 and 5. Notice that the displacements are as much as twice as large for the compacted soil arch, but subsequent live loading does not produce as much change. Both arches start with at-rest soil pressures, 2.5 times larger for the compacted soil, in the neutral position, but the soil load pushes the arch into a predominantly active position, particularly between the footings and the shoulders. This effect is larger for the compacted soil

because it has higher horizontal loads. The change caused by live loading is about the same for both the compacted and uncompacted soil assumption; in both cases the soil is starting from a similar horizontal pressure, because the soil load moved most of the forces to active, requiring similar deflections to increase the horizontal pressure to the lowest stable position.

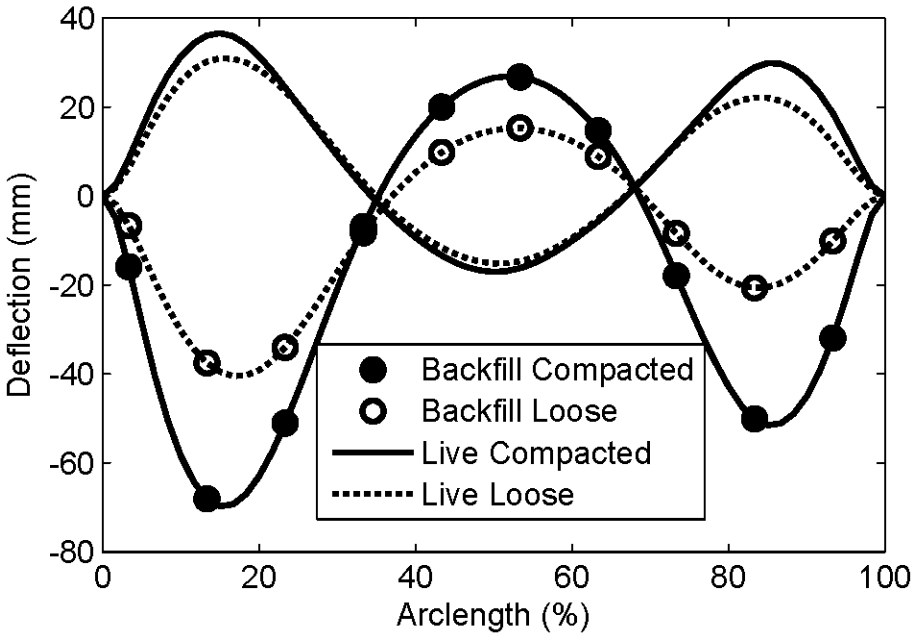

Figure 4. Deflection Behavior of Tall Arch, Compacted and Uncompacted

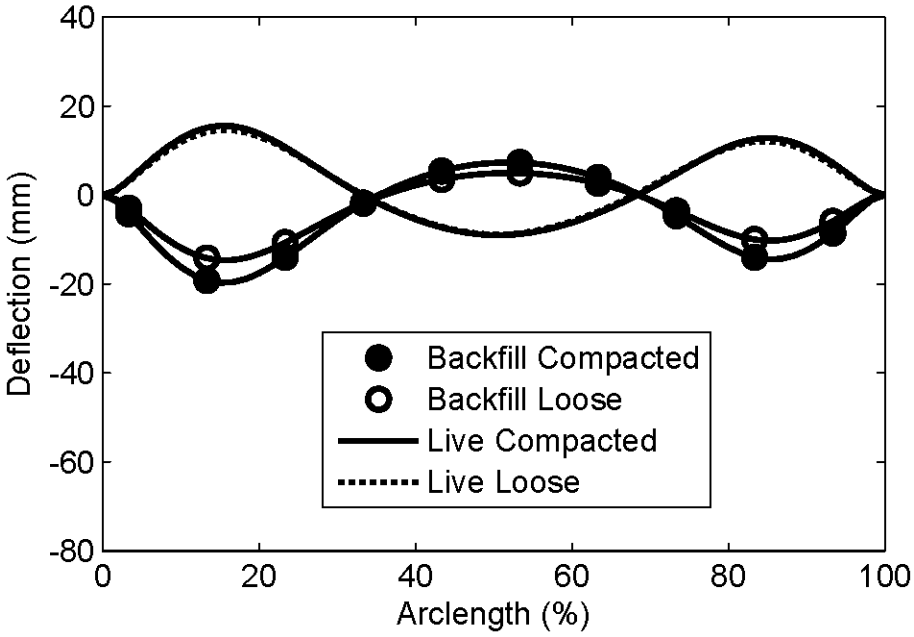

Figure 5. Deflection Behavior of Short Arch, Compacted and Uncompacted

FRP Properties

FRP properties are found using classical lamination theory for a thin multilayered plate. Classical Lamination Theory (CLT) with micromechanics was used to calculate the shear modulus and transverse (radial) and longitudinal moduli of the FRP shell (for further information on Classical Lamination Theory and micromechanics see Daniel and Ishai (2006)) by combining the properties of the fiber (carbon or glass) and the vinyl ester resin. For transverse modulus and shear modulus the Halpin-Tsai approximations were used (Daniel and Ishai, 2006). Fiber volume fraction was assumed to be 0.50. An additional complication is braid waviness; the braided fabric weaves over and under cross tows creating depth to the laminate inconsistent with the flat plate assumption; the 3D nature of the braid decreases the longitudinal modulus of the fiber. An approximation developed by Cox and Dadkhah (1995) based on a sinusoidal wave shape beam gives a longitudinal stiffness reduction factor. In Equation 1 t_f is the fiber thickness, λ is the

wavelength (measured at 18mm for the carbon), E_1 is the fiber elastic modulus in the fiber direction, G_{12} is the in-plane shear modulus, v_{12} is the Poisson's ratio. This model showed good agreement with results of coupon-level stiffness tests conducted at the University of Maine on carbon fiber only (Bannon 2009) and on hybrid glass and carbon composites (Demkowicz 2011), predicting modulus to within 10%.

$$E_1(wavy) = E_1\left(1+2\left(\frac{t_f\pi}{\lambda}\right)^2\left(\frac{E_1}{G_{12}}-2(1-\nu_{12})\right)\right) \qquad \text{Equation 1}$$

Typically, only the axial compliance matrix is considered for the hollow arches. Classical Lamination Theory assumes a thin composite plate; when that plate is instead a hollow circle the bending stiffness is greatly increased. Bending stiffness and combined bending/axial stiffness terms in the CLT compliance matrix are far too small when predicted assuming a flat plate, and the most accurate results are obtained by discarding the combined term all together and using the axial compliance matrix only to calculate the axial moduli.

The FRP shell is only a portion of the total stiffness; much of the arch stiffness comes from concrete. The concrete filled arch uses a model developed for concrete filled FRP tubes (Burgueno 1999), which assumes a Mander model (Mander 1988) for confined concrete. Concrete in tension is assumed cracked, a conservative assumption for strength design that under predicts bending stiffness and over predicts deflection. The level of cracking during any particular load cycle is difficult to ascertain because it depends on tensile stress in earlier load cycles, but the minimum bending stiffness occurs when concrete tensile strength is neglected. The Burgueno (1999) model also includes axial load; axial compression closes the cracks in concrete and increases the bending stiffness. Figure 6 contains a plot of the moment curvature relationship for a 300 mm arch with a variety of axial loads.

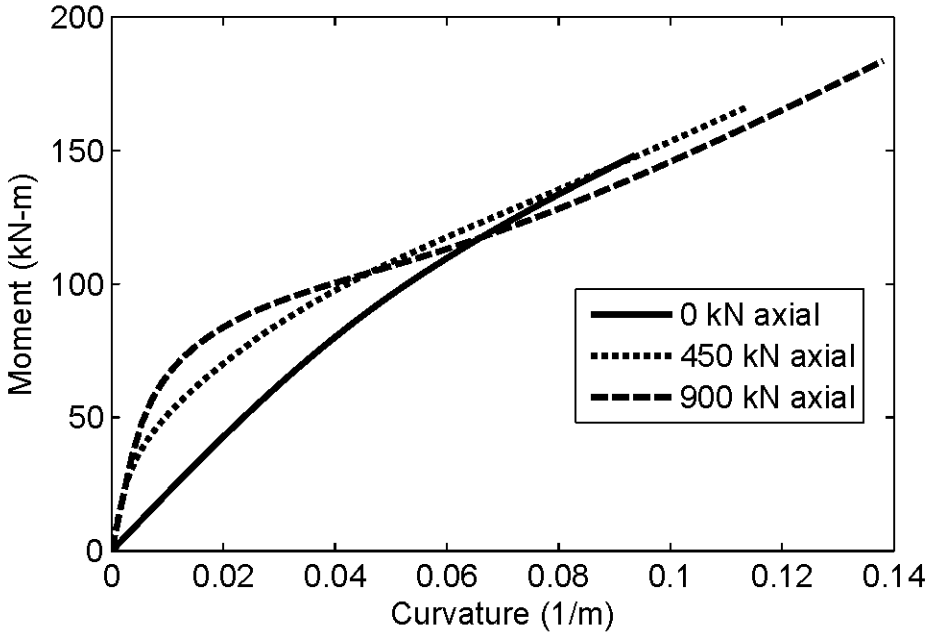

Figure 6. Moment-Curvature Relationship for a 300 mm Arch

Another source of axial stiffness in the system is the deck. Buried arch bridges constructed to-date have either a structural reinforced concrete deck or a structural FRP deck. The concrete deck provides noticeable axial stiffness; due to limited fasteners between the deck and the arch they are treated as separate entities without composite action. Deck stiffness is thus added to the arch stiffness at a given node. The FRP deck is much more compliant in the longitudinal direction and its stiffness is neglected. For subscale lab testing, a wood deck was used as explained later, which provides negligible longitudinal stiffness.

Scaling

Scale factor will be defined as the ratio of the full-scale bridge property to the equivalent subscale bridge property; e.g. for the 6.1 m span subscale of the 12.2 m assumed bridge the scale factor *S* for span is 2. The scaling objective was to maintain the same arch deflection while

keeping load distribution and the contribution from live and dead loads proportional; scaling terms for the relevant terms follow. Soil dead loads, per unit length, w_s are cross sectional area dependent, which means they vary by a factor of S^2 (4). When this equation gets integrated with respect to length the scale factor will increase by an additional S, e.g. shears and reactions have a factor S^3 (8), moments have S^4 (16), and deflections have S^6 (64). As a first estimate of mimicking deflection the bending stiffness of the section EI (elastic modulus E times moment of inertia I) was reduced by a factor of 64 in the subscale.

The full-scale bridge used as the standard in this study is a conglomeration of typical bridge dimensions and characteristics; it does not match the exact parameters of any existing bridge. By pushing a bridge to the arch moment and decking moment limits, as proposed by current design methodology, the soil effects will be maximized and there will be the greatest opportunity to see arch strains and deflections under equivalent service level loads. The standard arch used is a 12.2 m span at 1.5 m with a 1.22 m depth of cover at the crown, a rise of 2.44 m for the short arch 4.57 m for the tall arch 1.22 m by 1.22 m footings that continuously span between the arches, and a 300 mm diameter cross-section. The composite shell has three total layers: an innermost layer of +/-81degree, 1.1 mm thickness, E-glass inner layer and two +/-21 degree, 0.74 mm thickness, carbon fiber layers combined with vinyl ester resin and an assumed 50% fiber volume fraction (total thickness 2.5 mm). The elastic moduli, based on classical lamination theory and micromechanics, are 60 GPa longitudinal and 20 GPa transverse. The arches are filled with normal weight (2.3 Mg/m^3) concrete with a compressive strength of 35 MPa. The arches are covered with a reinforced concrete deck with properties based on a buried CFFT arch bridge built in Caribou, ME in 2011. The average deck thickness is 165 mm with minimum thickness 90mm, E is 26 GPa, I_{lp} (longitudinal positive) is 3250 mm^4/mm, I_{ln} (longitudinal negative) is 1080 mm^4/mm, I_t (transverse positive) is 52400 mm^4/mm.

Scaling the FRP Arch

The subscale FRP arch diameter cannot be half of the diameter of the larger arch; the shell stiffness and core stiffness vary with a different scale than deflection. Deflection varies with S^6, while I for the core varies with d^4 (the cracked concrete is not linear elastic – I is not valid, but it is a useful starting point), core area varies with d^2 (important because crack closing and bending stiffness depend on axial stress), and I for the shell and section modulus for the concrete vary with d^3. Using I for the core as the determining factor the diameter would be 107 mm; axial stress has the same scale factor. Nonlinear behavior changes the stiffness considerably; the concrete bending stiffness is more dependent on crack depth and estimated section loss than gross moment of inertia. If diameter were scaled by moment, scale factor 16, over section modulus, d^3, the required diameter is 120 mm. To compromise on these relationships the diameter was specified as 114 mm. Ideally, if all parameters were scalable, the crack depth should be identical for the subscale and the full-scale arch, but the required compromise between bending stress and deflection means that the crack depths are not identical and the difference is compensated with the transverse shell stiffness. Additional alteration allowed by changing the concrete density only slightly change the response of the arch, but changing the concrete strength has multiple effects: it reduces the elastic modulus of the concrete and it changes the strength analysis altering the crack depth and the stiffness of the section.

The shell is linear elastic; to reduce the number of differences in the scaling process the shell bending stiffness should also be scaled. It is impossible to scale the shell thickness; a certain thickness per layer is required to maintain transverse strength and stiffness and keep fiber coverage for the part. Based on the cube of the relative diameter, the reduction of longitudinal stiffness, E_x-t, is slightly over 3.5. The total longitudinal elastic modulus E_x for the full-scale section based on CLT is 50 GPa and shell thickness t is 2.5 mm; longitudinal stiffness E_x-t is 130 kN/mm making the required subscale E_x-t 36 KN/mm. The lower longitudinal stiffness requires

only a single outer layer of E-glass fiber reducing the thickness and the modulus while improving cost, manufacturability, and strain to failure. There are several different possible combinations of fiber angle and material thickness for both layers to produce the required longitudinal shell stiffness.

The shell was also designed to provide the correct confinement capability. Confinement pressure comes from the hoop stiffness of the shell wall E_r-t. At low curvatures the confinement contribution to the moment-curvature relationship is quite small, overwhelmed by other section parameters, but as the concrete is more cracked the transverse shell stiffness, which holds the cracked concrete together, noticeably affecting bending stiffness. To scale the response, the confinement potential was also scaled with the inverse of the discrepancy between theoretical and actual gross concrete moment of inertia. Because the compromised diameter produces a 30% smaller concrete I than the theoretical value, a 30% smaller confining pressure was needed to adjust the bending stiffness of the subscale for high strains. E_y-t for the full-scale arch is 50 kN/mm, scaled for the subscale's response it is 39 kN/mm.

The laminate chosen, using CLT and micromechanics, was an inner layer of E-glass +/-75 degrees, 1.0 mm thickness, and an outer layer of E-glass +/- 25 degrees, 0.89 mm thickness, with total thickness 1.9 mm and elastic moduli E_x of 19 GPa and E_y of 20 GPa. Micromechanics predictions can be accurate to within 10% for braided hybrid glass/carbon composites (Bannon 2009), but coupon level testing was performed to obtain better predictions which were unavailable when designing the test. Concrete strength can be slightly adjusted to change the moment-curvature relationship if the laminate proves to be either substantially stiffer or more flexible than predicted.

The moment-curvature relationship was calculated using the Mander (Mander 1988) model for confined concrete, using a program developed by Burgueno (1999). The same approach has been used to successfully model the bending response of carbon-glass hybrid CFFTs (Bannon

2009; Dagher et al 2012). This model uses a given axial stress and the previous outlined material properties for inputs. The model starts with compressive strain. It finds compressive stress based on the material properties and then finds the appropriate tensile stress and strain to balance the axial load. The stresses are used to compute moment and the strains are used to compute curvature. In the arch model the Burgueno moment-curvature relationship is precalculated and stored for several axial loads. For a given moment and axial load the curvature is linearly interpolated from the precalculated values. Bending stiffness (tangent modulus) is the local moment divided by curvature; this is calculated for each node.

Scaling the Steel Arch

One major advantage to using steel arches is that steel is linearly elastic, meaning the arches (not the soil) will rebound so long as stress does not exceed the yield limit. Steel is also easy to instrument. The process of matching deflection to determine the steel section will be described in more detail later. Strength is a major issue for the steel arches; an HSS (hollow structural steel) or pipe section would be an efficient section for bending to an arch shape, but the required yield capacity dictates a prohibitively large section modulus of 25000 mm^3 for 290 MPa steel; any section with a capacity near this limit was too stiff. To correct this, additional steel was needed near the neutral axis, suggesting a steel plate, which is materially inefficient for bending, but does provide a high bending strength to bending stiffness ratio. Plates were sized for both grade 36 (250 MPa) and 50 (344 MPa) steel, but grade 50 steel will have a smaller section with a more reasonable width.

Decking

The decking in arch bridges built prior to the design of this testing program is 200 mm thick concrete (maximum thickness) with #5 bars at 200 mm on center in the transverse direction and #3 bars at 400 mm on center in the longitudinal direction. The concrete deck is supported during

casting by a corrugated FRP deck. The assumed decking has a 200 mm. The decking is not symmetric. Figure 7 has a section view of the decking by Matthew Pellerin of AIT (Clapp and Davids, 2011). The transverse direction runs into and out of the page.

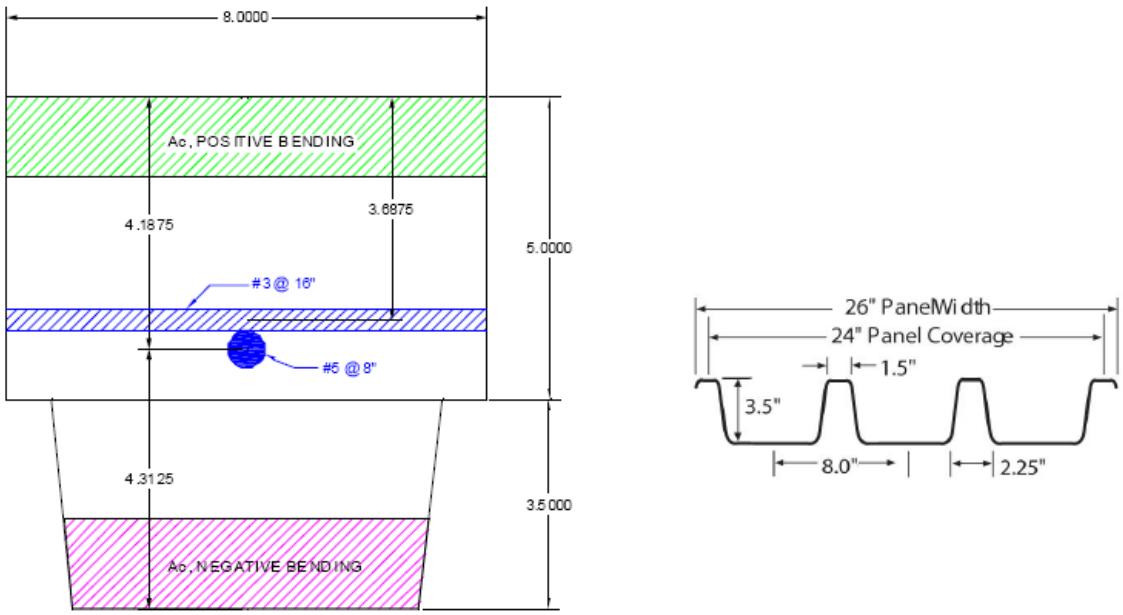

Figure 7. Decking Cross-Section (provided by AIT)

The transverse response of the decking was scaled, and no longitudinal effect of the deck was considered in the subscale model. Decking for central arches, those that carry truck and lane loads, is designed as an infinite continuous beam. With only three arches, and thus two inner spans, decking deflection is influenced by the response of the two cantilever spans outside the arches; to keep inner deflections consistent the outer decking cantilevers should generate the same moment as an additional decking span. To keep zero rotation in the decking above the arches, the moment at the cantilever edge must equal the moment in the continuous span. For simplicity, soil and traffic loads are treated as a uniform load. The moment at the fixed end of a uniform loaded cantilever is $wl^2/2$, while the moment at the end of a continuous span is $wl^2/12$. The scaled length for the continuous beam is 760 mm; to produce the same moment the cantilever span should be 310 mm.

Transverse deck stiffness must be represented in the subscale test. The concrete deck assumes transverse #5 bars at 200 mm on center slightly above the central height of the section. The top width per bar is 200 mm and the FRP decking corrugations make the bottom width per bar 155 mm. For a fully cracked section assuming the Whitney stress block and a maximum compressive strain of 0.003, both sections have a similar *I* which can be rounded to two significant figures to 52000 mm^4/mm. To get the same deck deflections with the subscale as with the full-scale the bending stiffness of the arches should be reduced by one-64^{th}, however width is already scaled by one half; scale factor was one-32^{nd}. *EI* for the full-scale arch deck is 2120 kN/mm; required *EI* is 66 kN/mm. This is too soft for a concrete deck, and FRP decks are expensive; a wooden deck, using a combination of flat-wise studs and sheathing, is inexpensive and can have the same bending stiffness. SPF-s (spruce, pine, fir – south) has longitudinal elastic modulus 8.3 GPa, and flat-wise 2x lumber has *I* equal to 4600 mm^4/mm. *EI* for continuous lumber is 60 kN/mm and additional stiffness is required. Adding a ¾ in nominal plywood sheet adds 4.4 kN/mm (APA) assuming a non-composite section, a composite section would be higher. This stiffness is adequate to mimic the decking behavior.

Two decking effects were not imitated in the subscale: the additional weight of the concrete deck and the longitudinal stiffness of the concrete deck. The surface area of the concrete deck is scaled with soil volume, but the 165 mm mean thickness and 2.4 Mg/m^3 density of reinforced concrete are not scaled by using 57 mm pine, with 0.36 Mg/m^3 density. The additional weight does not cause much deflection because it is uniform over the arch; it does not initiate soil springs because soil is not yet placed when the deck is cast. The additional stiffness is small because longitudinal reinforcing is a #3 bar spaced at 400 mm on center; it is also not symmetric, because the deck runs opposite the corrugations, and the concrete inside the troughs is neglected for longitudinal analysis. The cracked positive longitudinal moment of inertia is nine times larger than the cracked negative moment of inertia. During analysis, this property is directly added to

the arch stiffness, and while small compared to the arch stiffness, it is another difference between full scale and subscale analyses.

Load

There are two main sources of load: soil dead load and truck live load. Soil dead load was scaled with volume, and the magnitude of the live load is scaled by the same ratio: one to eight. Surface live loads are distributed through the soil using the Boussinesq assumption for a patch load (Holtz and Kovacs 1981), which requires a patch size and shape. AASHTO (2011) defines a truck tire patch (from a wheel load) as being a uniformly loaded rectangle of area 25 mm x 50 mm. For the subscale patch the dimensions are scaled by one-half, the same ratio as the span. For design, AASHTO requires both the HL-93 truck and tandem. Although the HL-93 design truck has higher wheel loads, the tandem has smaller spacing and often controls design for short span bridges, including buried concrete filled FRP bridges. In this program the tandem is the only truck considered, and further reference to a truck's load refers to the tandem's load. The tandem is a 224 kN vehicle with two axles spaced at 1200 mm with a 1800 mm axle width. The State of Maine also requires a 25% capacity increase on the HL-93 truck and tandem, which was included in the model. All models are run with the load of the HL-93 tandem, plus the Maine 25% increase, plus an additional 20% increase to account for overloaded trucks, similar to the multiple presence factor. Impact is not included in this analysis because laboratory loading will not be dynamic and impact is reduced on buried structures. All models have service level loads; service loads will be applied to the lab experiment to find appropriate deflection. In design, service loads are applied to the bridge to find deflections and handle nonlinear behavior; the loads are scaled with strength factors after to verify capacity.

For laboratory testing, it was deemed impractical to apply the four patch loads required for true AASHTO specified tandem loading. Models were made for the truck either as two line loads, one representing each axle, or a single combined line load that concentrated the full weight of the tandem. The line load uniformly spanned all three arches. For the full scale 300 mm arch, Figure 8 (tall arch) and Figure 9 (short arch) compare the model predicted moments for the center of three arches with the assumed loading from the four tandem patches, the two axle lines, or the concentrated line, all straddling the arch apex. The moments are very similar, indicating that there is little difference between the three loading cases. The single line load makes the moment more positive at the point of load, and the difference is more pronounced in the short arch.

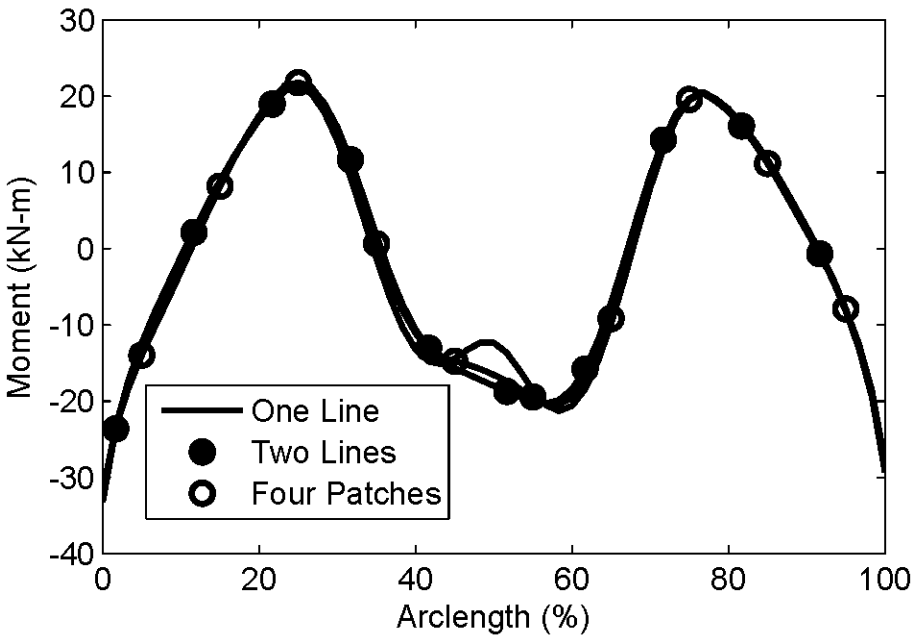

Figure 8. Tall Arch Moment from Different Truck Models

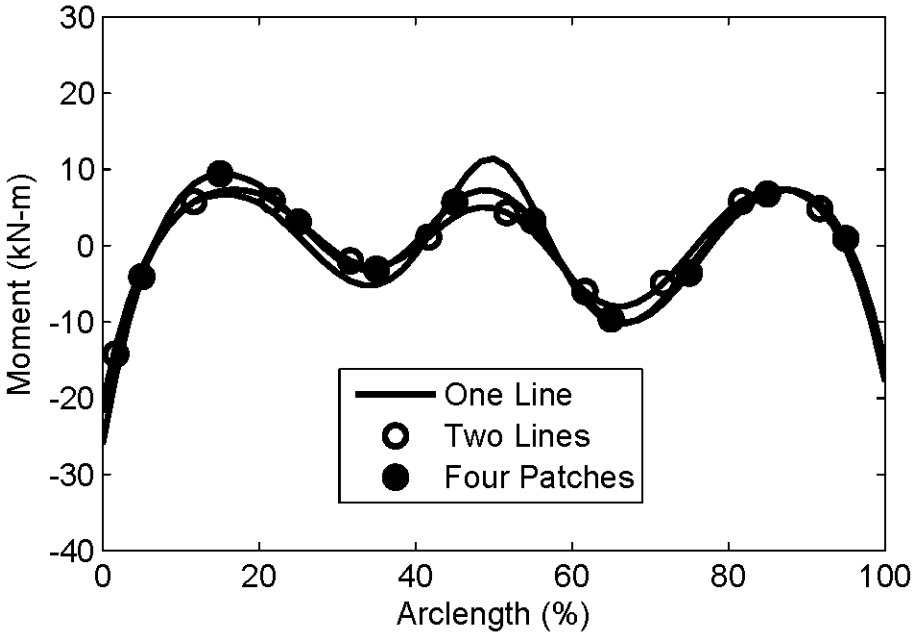

Figure 9. Short Arch Moment from Different Truck Models

The bridge will be loaded with the simulated tandem in multiple locations. Four different loading plans were proposed and the arch moment envelope for each plan was compared for both the two line loads and the single line load. Options included loading the arches over the entire span at 300 mm and 600 mm intervals, or loading the center 60% at 300 mm and 600 mm intervals. Testing time and logistics are important; each load position requires moving the actuator and possibly the reaction frame, not a trivial process, and the laboratory floor has holes at 600 mm intervals giving a strong bias to testing at that spacing interval. Figure 10 and Figure 11 contain the live load moments for subscale linear elastic steel arches applying two line loads. Notice that peak moments are still well represented by applying load at 600 mm intervals over the middle 60% of the span when compared to applying load at 300 mm intervals. The load over the outer 20% of span on either side appears insignificant; the moments in those regions are not strongly influenced by a direct vertical load and are smaller than live load moment above the shoulders and the apex. Also notice that the peak moment is more consistent over the middle 60% using 300 mm loading interval, but there are still many locations where peak moment is the same

for both loading conditions. This justifies that there will be opportunities to measure high live load using either load plan, which favors the substantially simpler 600 mm intervals over the middle 60% of the span.

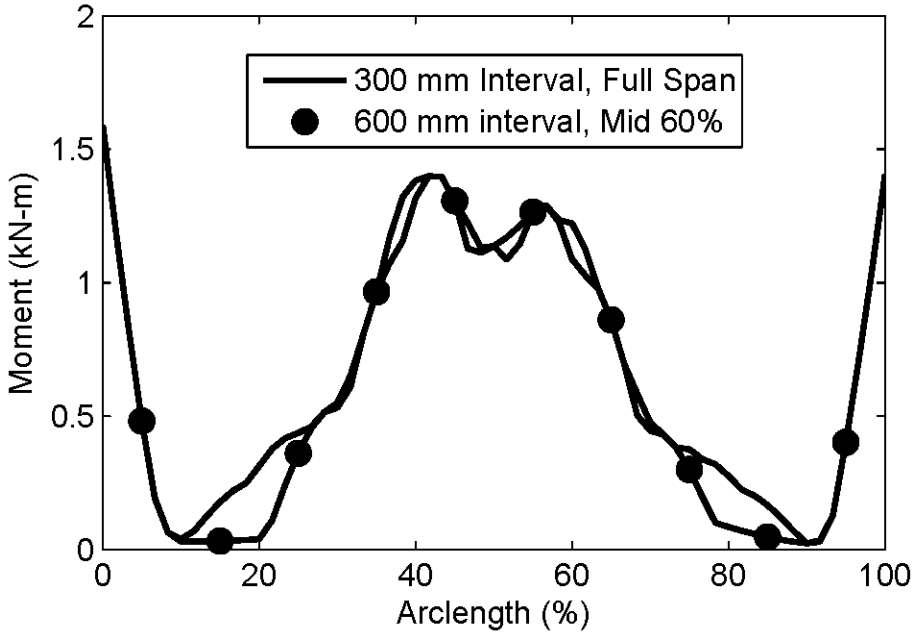

Figure 10. Tall steel arch, positive moment envelope

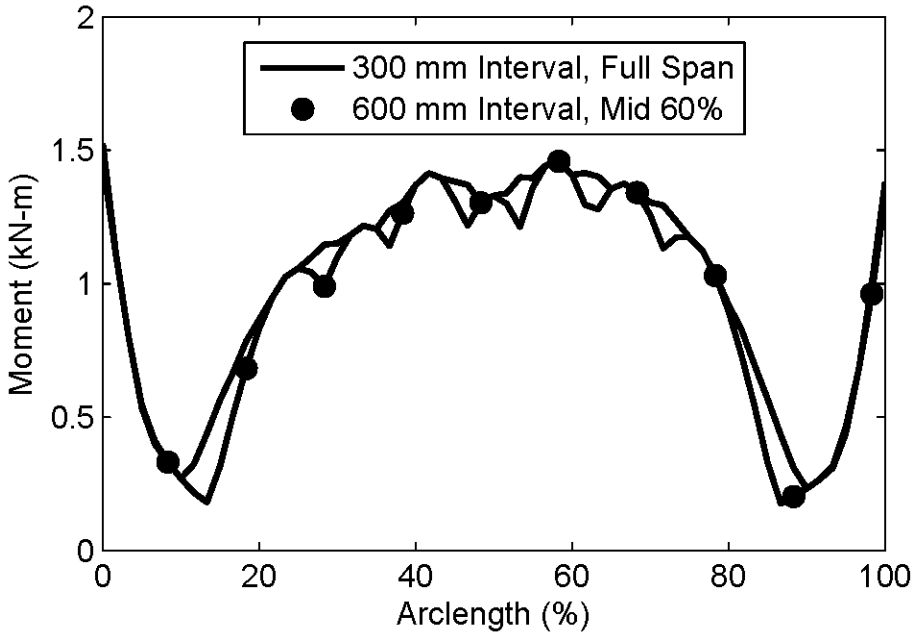

Figure 11. Short steel arch, positive moment envelope

A second consideration is whether to apply load as a single concentrated load or as two line loads. Two line loads are more representative of bridge loading by a design tandem with two axles, but single line loading is preferable for testing logistics. Figure 12 and Figure 13 contain plots illustrating positive live load only moment envelopes for one and two line loading for both the tall and short linear elastic steel bridges. The load case depicted is middle 60% of span loading with 600 mm spacing. Notice that in both plots the one line loading envelope is higher for any location than the two line loading envelope, by as much as 40% in local maxima locations. Testing at a higher moment will give better resolution to gauges and improve model to laboratory experiment comparisons. Note: the envelopes are not symmetric because soil compaction occurs on one side at a time starting with the right side.

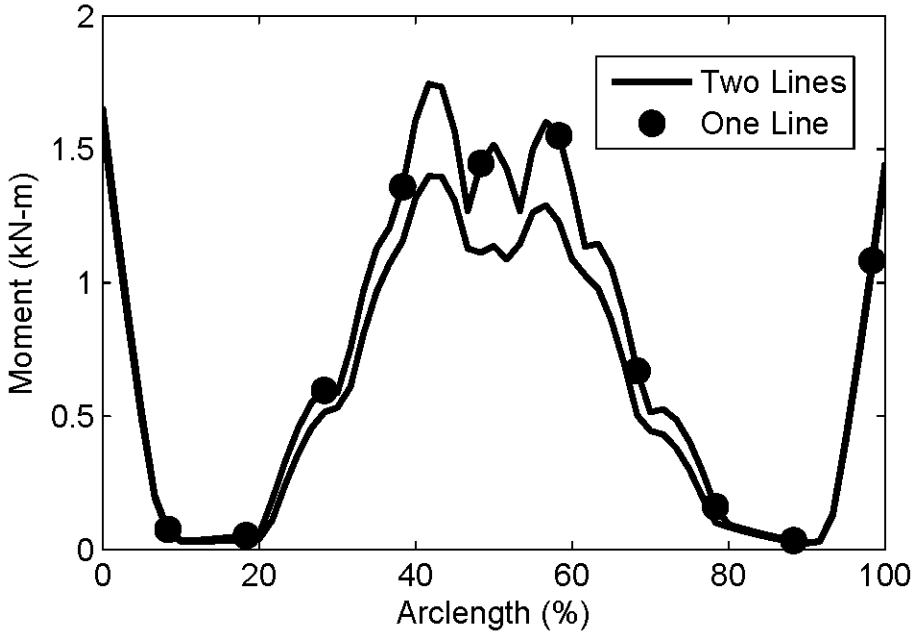

Figure 12. Tall steel arch, moment envelope for one and two line loading

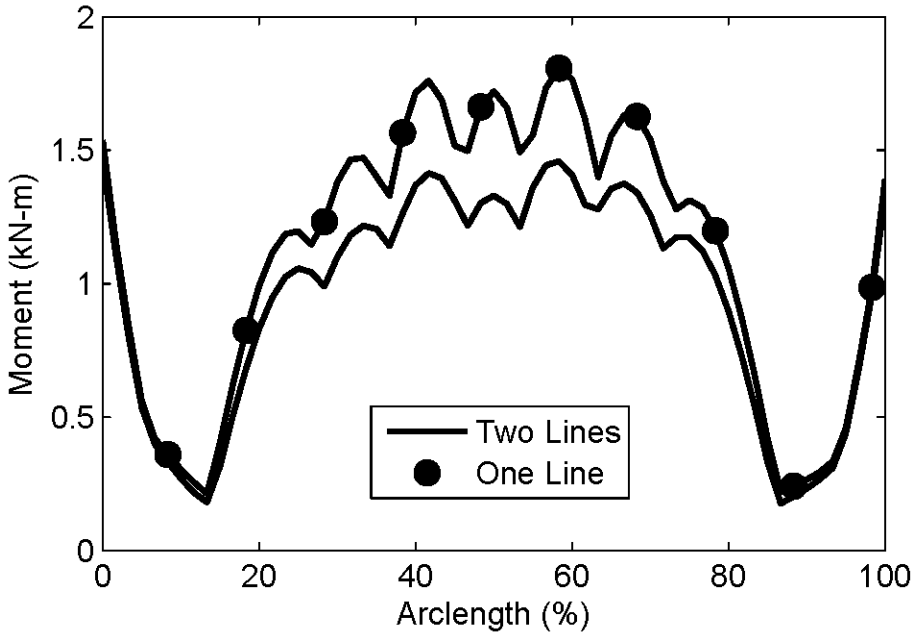

Figure 13. Short steel arch, moment envelope for one and two line loading

Strength

The arches cannot fail during backfill or service loading, yet there must be enough actuator capacity to fail the arches during ultimate loading. For a concrete filled FRP arch the most likely failure mechanism is tensile fiber rupture. Because glass fiber is used for the longitudinal strength layer, and it typically has a higher strain to failure than carbon fiber, additional failure mode transverse fiber rupture (confining strength) is more likely. Longitudinal strain capacity was estimated from coupon testing for a new glass fiber lay-up from AIT (AIT 2011), giving a strain to failure of 1.85%. Based on an appropriately high axial compressive load, the Burgueno model gives a failure moment of 9.6 kN-m; this value is dependent on axial load, but does not vary much in the critical axial range (130-200 kN). Coupon testing prior to full arch testing will better estimate tensile rupture strain. Hoop strain failure was also estimated at 1.85%; for this failure, the Burgueno model predicts a failure moment of 15.8kN-m; the tensile failure is more likely, but these values are estimates and it is possible that the arch is stronger or weaker than anticipated. All loads calculated in this analysis are service level, not strength level; a factor of safety was calculated for each arch during backfill and live load. Figures 14 and 15 show the moment envelopes for soil backfill the 600 mm interval mid 60%, single line live load envelope for the tall and short arch respectively. The soil backfill creates the largest moment in the load history of the tall arch; approximately 5 kN-m at the right footing. The subsequent live loading produces larger moments at the shoulders and the apex, positive 2.6 kN-m and negative 3.7 kN-m respectively. For the short arch the soil backfill moments are smaller; the largest moment is during live loading at the apex, near 4.5 kN-m. In all cases the moments are small compared to the projected failure moment of between 9.6 kN-m and 15.8 kN-m, providing approximately a factor of safety of 2 for both arch geometries.

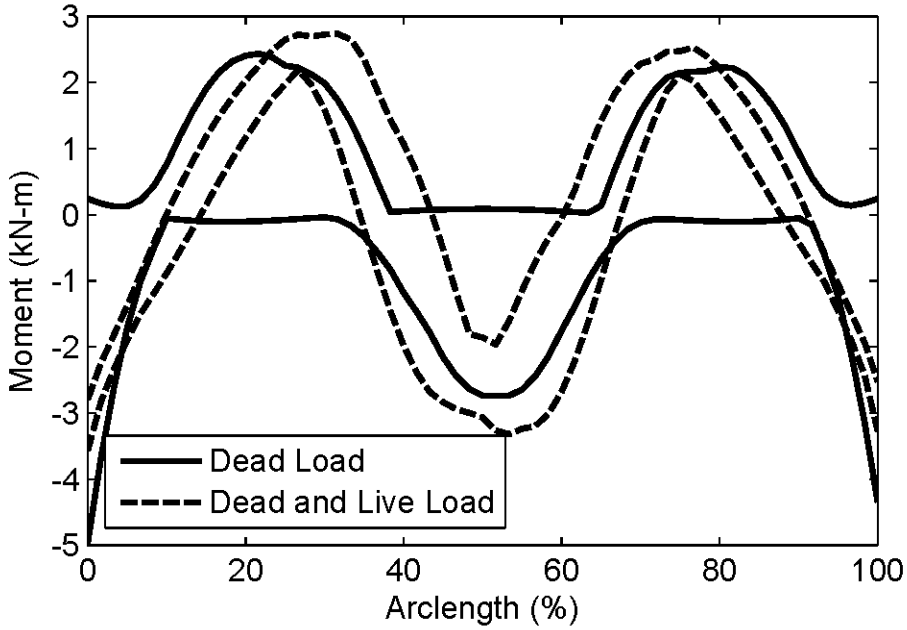

Figure 14. Dead load envelope and dead plus live load envelope, tall FRP arch

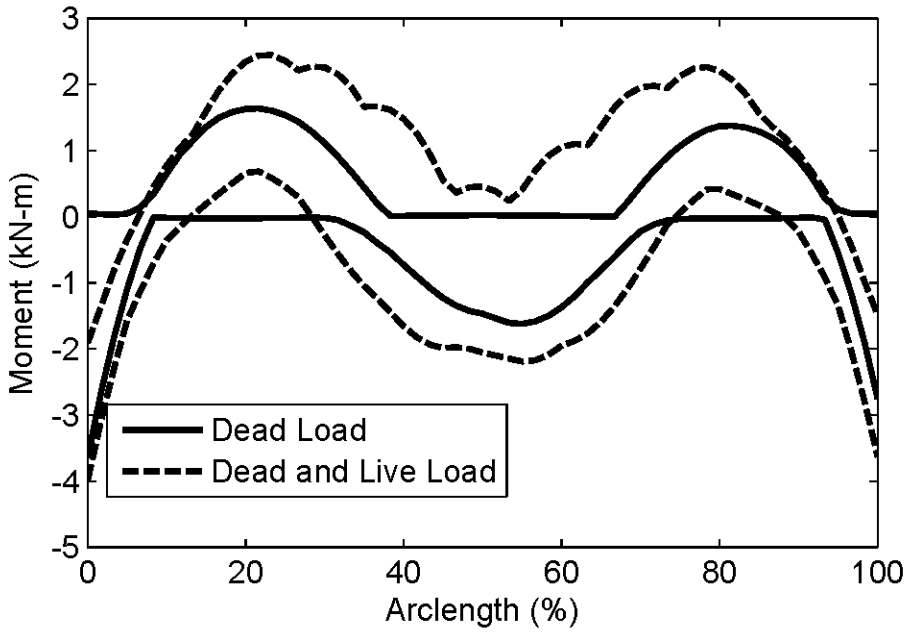

Figure 15. Dead load envelope and dead plus live load envelope, short FRP arch

Soil pushing at the sides of the arches from partial soil depth causes the arches to rotate inward and generates negative moment on the footing (tension on the outside face). The peak footing moments are generated when the soil depth is level with the arch apex. Load applied to the arch apex deforms the arch into an ‘m’ shape, causing positive moment at the footings, reducing the effects of earlier backfill. Failure at the footing, generating a plastic hinge at the footing, would not necessarily fail the system, but would invalidate all following results because bridges in service retain a fixed footing to arch connection.

For steel arches, yielding at any point during the test would invalidate the assumption that the material is linear elastic. The steel arches are designed for appropriate stiffness and adequate strength with an appropriate factor of safety. Stiffness adequacy was determined by minimizing the difference in the scaled horizontal soil pressure between the full scale and the steel subscale. The optimal moment of inertia was approximately 460,000 mm^4 tall arch and 580,000 mm4 short arch. The steel arches have similar internal moments to the FRP subscale: maximum moments are 5 kN-m and 4.2 kN-m for the tall and short arch respectively. Arches are designed to have a safety factor of 1.5 against the start of yield. Axial load only uses 14 MPa or less of the steel’s capacity due to the large steel area and the relatively small axial loads. Assuming grade 50 steel (345 MPa) the required section modulus was 23,000 mm3 for the tall arch and 20,000 mm3 for the short arch; the best sections were a 1.5x4 (38 mm x 102 mm) bar stock for the tall arch and a 2x2 (51 mm x 51 mm) bar stock for the short arch (both dimensions are common manufactured bar sections). Hollow Structural Steel (HSS) is manufactured from 290 MPa steel (round) or 317 MPa steel (rectangular) and the axial arch stresses are higher because there is less area The tall arch cannot be manufactured from a hollow section, because the required section modulus is too large relative to the moment of inertia, but the short arch could be manufactured from a rectangular section HSS 4x2x1/2 (102 mm x 51 mm x 26 mm) that uses the section’s weak axis in

the vertical direction. This option uses approximately half the steel of the 2x2 bar stock and may be economical, although the section may warp during arch shaping.

Arch failure for this research does not correspond to collapse of the arch but to inelastic behavior: the entire point of a steel arch to find soil-structure interaction without material nonlinearity. If the arch begins to yield there should be considerable reserve capacity before collapse. A plastic hinge should form at 50% greater moment (for a rectangular section) than the onset of yield, and even a single hinge should not cause collapse of the system: each arch is 3rd degree indeterminate, and can support two hinges before collapse. Once one arch yields the other two arches, which are connected with the decking, will share the load from the damaged arch. The soil will also carry more load once the arch yields due to decreased arch stiffness.

After completing the suite of live load tests it will also be important to find the ultimate system capacity. Load will be applied as a line across the apex until the arches fail. Ultimate load was estimated iteratively; load was applied to the apex until the moment exceeded the moment capacity for the arches; 9.6 kN-m to 15.8 kN-m for 115 mm concrete-filled FRP arches. The model predicted a failure load of 300 to 400 kN for the tall arch and 230 to 300 kN for the short arch. In both cases the capacity might exceed a single 250 kN actuator and it will be necessary to run two 250 kN actuators in tandem or a single 500 kN actuator, although this may not be possible due to space limitations. The failure analysis is also less accurate than other analyses; as load increases the soil plays a larger role and any error in soil behavior will be magnified. Despite loading a generous area, the 400 kN vertical load will apply 1200 kPa pressure under the load beam and this pressure is likely to fail the soil, or at last cause excessive deformations that further concentrate the load.

Decking strength is a concern. Decking was evaluated based on the National Design Specification for Wood Construction (American Forest & Paper Association, 2006). This standard is based on allowable service loads; no load factors were required for analysis. In a very

conservative assumption the plywood was ignored in analysis; this will under represent the total decking capacity. Two areas of concern are the dead load pressure near the footing and the live load pressure at the apex during ultimate load. The footing does not see much live load and the apex has little dead load. Allowable bending stress for #2 SPF-s is 5.3 MPa, but when flat use, repetitive member, shape, and load duration factors are considered the long-term capacity (month – dead load) is 11.6 MPa and the short-term capacity (10 min – ultimate load) is 16.2 MPa. Weak axis section modulus per unit width is 240 mm^3/mm; failure moment is 71 N-m. For compacted soil the horizontal pressure coefficient *K* can be taken as 1.0 at-rest (the footing does not move, soil is at-rest near the footing), the same as the vertical pressure. The stud will therefore have pressure equal to the weight of the soil above in the weak axis direction regardless of the orientation of the stud. Max moment is 70 N-m from 2.9 m of soil in the tall arch, below the allowable moment. Ultimate load decking force was taken as the point-applied gravity load at the apex node from analysis, 10 kN over a 0.10 m^2 tributary area. Also, the load is calculated assuming the soil does not deform; soil deformation will reduce the cover and reduce load propagation through the soil. The decking moment is 121 N-m, above the 70 N-m capacity of the lumber. Without the composite action the sheathing will still add some capacity, but for added safety an additional 2x4 above the sheathing bolted onto the 2x4 below will give enough capacity, without composite action, to meet the load requirements. Away from the load source it is unlikely that the decking will fail, since vertical soil pressures drop rapidly.

Verification of Horizontal Pressure

The goal of this study is to determine soil structure interaction for a buried structure by mimicking the horizontal soil pressure for a scaled structure and testing it in the lab. As stated previously the most important horizontal soil pressure is the change, after considering the dead load pressures, caused by an apex live load. Horizontal soil load is calculated per node and is

generated using tributary area assumptions. Nodes closer to the apex have smaller vertical areas and less vertical overburden and therefore have less potential to generate horizontal soil loads, while nodes closer to the footings have larger areas and more overburden, generating larger horizontal soil loads. In the transition from dead load only to dead plus live load, as shown in Figures 16-19, the nodes near the apex become more active, but the large increase in overburden pressure still causes a large pressure spike on the arches. Nodes closer to the shoulders deflect into the soil transitioning from active pressures to at-rest or even passive pressures, which generate a greater soil pressure. Near the footings the arches do not change horizontal soil pressure much, but the increase in horizontal load is still relatively high because of larger vertical tributary areas.

Change in pressure is compared at all points: the square root of the sum of the square of the difference between the target pressure and the subscale pressure (scaled by a factor of 2) divided by the sum of the target pressure. If this error term is zero, the numbers are identical and if error is greater than 1, the subscale model fits worse than zero pressure. The computed error can be deceptive; simulations that are divergent in only a couple of points can show a large error even if many of the points are close. Small pressure changes, near zero, have little weight; good approximations of low values do not help the error estimate. For example, the computed error is 0.324 for the 115 mm subscale depicted in Figure 16, but 30% of the error comes near the far shoulder (5 nodes, 8% of the span) where the subscale's peak is higher and the secondary peak is off by a couple nodes. For the short arch in Figure 17 the fit is slightly better; the error was 0.281. Most of the error was at the shoulders as the full-scale model distributes pressure over a greater percentage of the arclength. This is ultimately still a reasonable fit.

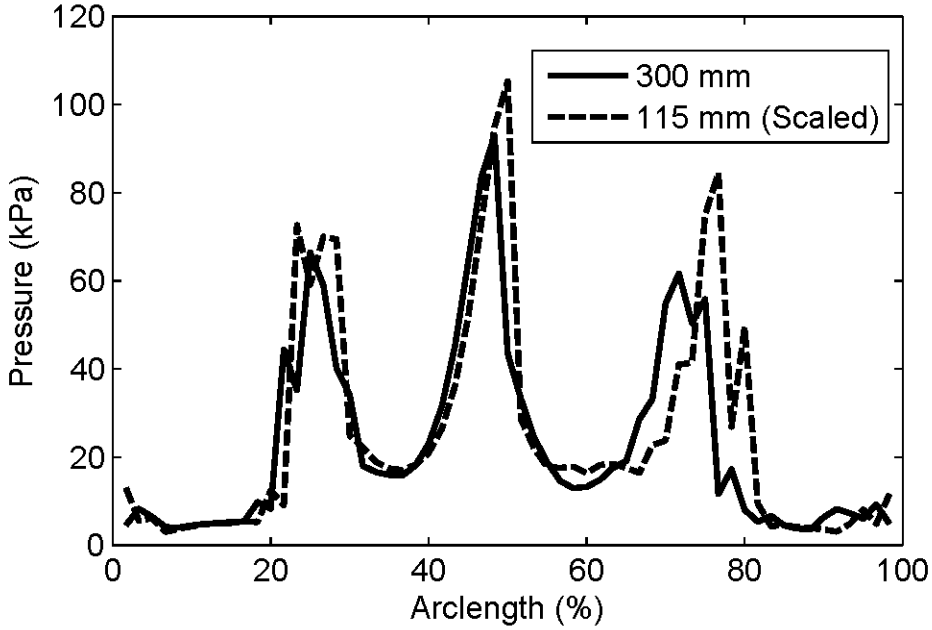

Figure 16. Scaled Change in Horizontal Pressure, Tall

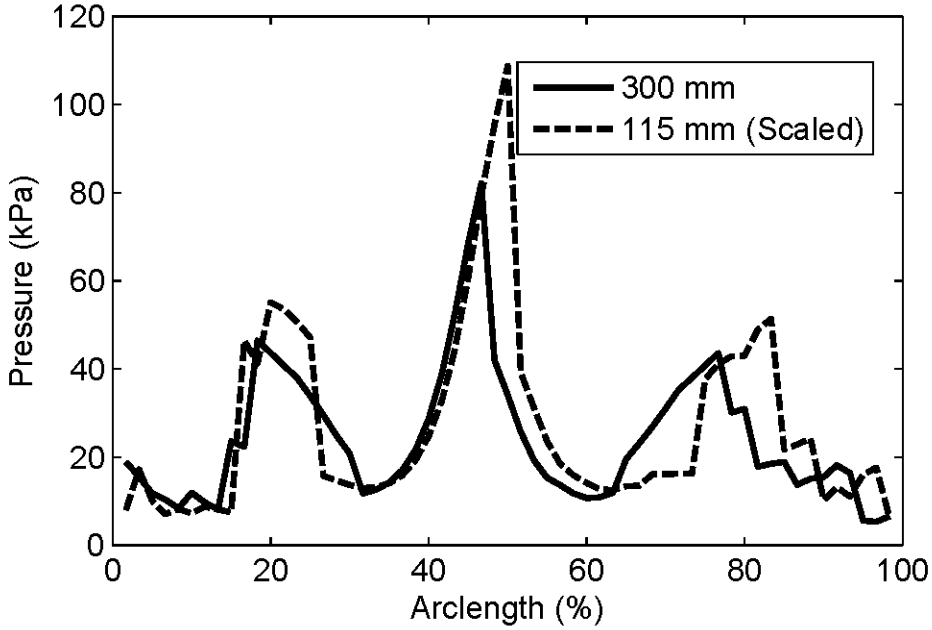

Figure 17. Scaled Change in Horizontal Pressure, Short

Overall, there was very little change to the horizontal soil pressure when the moment curvature relationship changed for the concrete arches. Changing the concrete strength has more effect on backfilling deflections, but minimal effects on deflections and horizontal pressures caused by apex load. Figure 18 shows the pressure difference for 34 MPa and a low strength 10 MPa concrete subscale tall arch. The lower strength concrete does behave more similar to the full-scale, with an error of 0.255, but there are additional effects with changing the concrete mix, such as shrinkage and flowability, which outweigh the small improvement in replication.

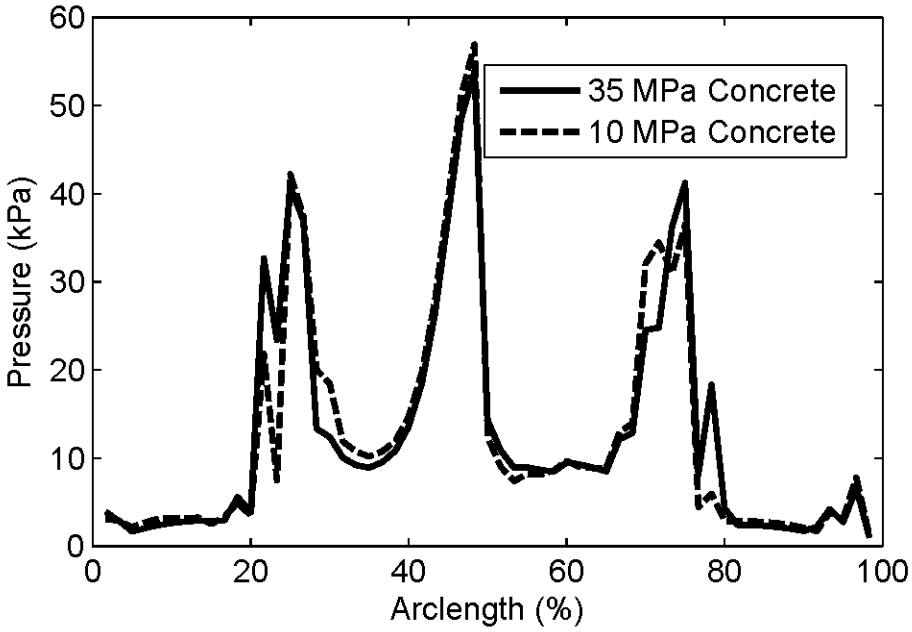

Figure 17. Horizontal Soil Pressure with Different Concrete Strengths

The steel arches were sized specifically to reproduce the horizontal soil pressures of the full-scale arches by varying the bending stiffness. No stiffness will be a good fit for all nodes; the selected section had the minimum value for any common bar stock section (in 50ksi). For the tall arch the fit is remarkably good; error was 0.075, and Figure 18 displays how close the values fit. For the short arch the fit was worse, error was 0.248, and Figure 19 displays this comparison. The

fit could be improved by using a slightly higher moment of inertia, closer to 620,000 mm^3 instead of 550,000 mm^4, but there are no common bar stocks that are near that size, a 1.5x5.5 (38 mm x 140 mm) would give a better fit than the 2x2 (51 mm x 51 mm), but that is a custom section and requires double the steel area. The selected shape does have a similar error to the FRP subscale and is a reasonable solution. Alternatively, an HSS4x2x0.5 rectangular section, in weak access bending, also produces a better fit if it does not change shape during bending.

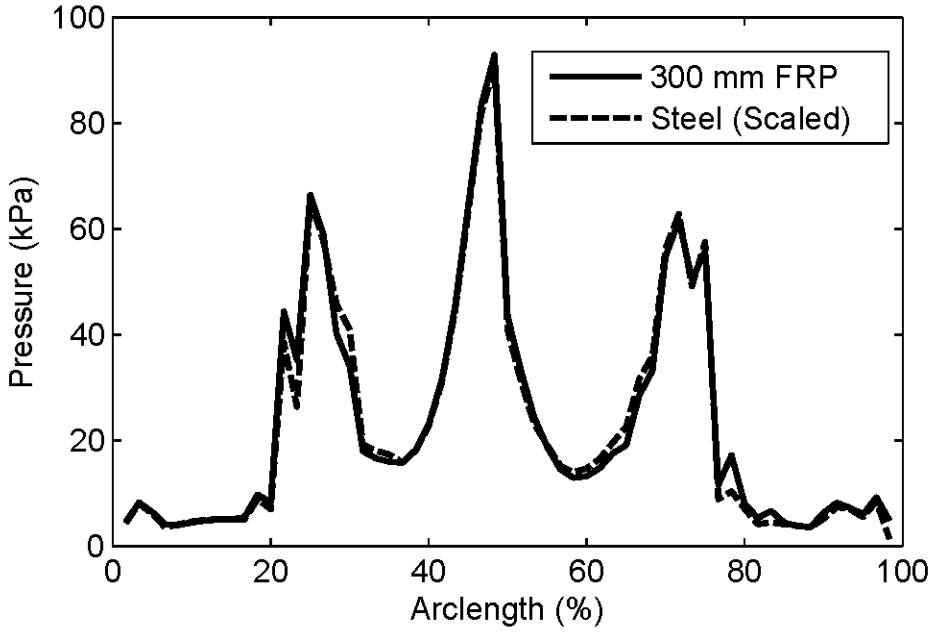

Figure 18. Tall Arch, Steel Comparison

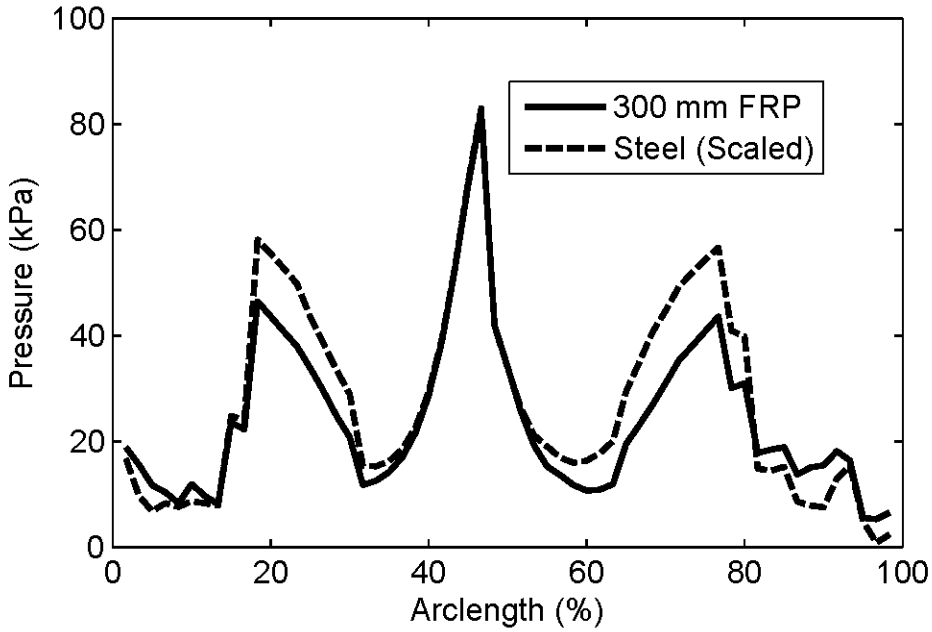

Figure 19. Short Arch, Steel Comparison

Horizontal soil pressure can be deceptive near the apex and footings. The model does not include soil springs at either the footings or the apex because the model footings are fixed against horizontal translation and any force corresponding to a fixed degree of freedom will be zeroed. The apex does not have a node because the apex has virtually no vertical tributary area; regardless of how large the horizontal pressure, it would not apply a horizontal force in the model. Similarly, the large spike in horizontal pressure at the apex of the model due to applied live load does not create a large spike in horizontal force. The horizontal forces of the nodes near the center remain modest compared to the forces near the footings and shoulders sue to the relative vertical area.

Conclusions

By mimicking the moment-curvature relationship of the FRP arches there is a reasonable approximation of horizontal soil pressures. While further decreasing the arch stiffness produces a

better fit to horizontal pressure, it comes at a price to manufacturability, structural similarity to the full-scale arch, and may compromise structural capacity needed in the testing program. A consequence of this scaling is a loss in deflection matching; the subscale arches must deflect less than the full scale arches to generate the same horizontal pressures, and this is unconditionally true if soil stiffness and load are dependent on the height of the arch.

Steel sections are limited primarily by strength and availability. For 345 MPa steel, sections were selected that are hot-rolled bar shapes, although they could be cut from plates. A 345 MPa 1.5x4 bar stock (38 mm by 102 mm) weak axis was used for the tall steel bridge and a 345 MPa 2x2 bar stock (51 mm square) was used for the short steel bridge.

References

AASHTO. (2014). LRFD Bridge design specifications, 7th Ed., AASHTO, Washington D.C.

AIT (2011). [AIT REPORT FROM KEENAN – FIND?].

APA (1998). *Plywood design specifications*. Engineered Wood Association, Tacoma, WA.

Barker, R.M., Duncan, J.M., Rojiani, K.B., Ooi, P.S.K., Tan, C.K., Kim, S.G. (1991). "*NCHRP 343: Manuals for the design of bridge foundations*." Transportation Research Board, Washington D.C.

Bannon, D. (2009). Characterization of concrete-filled fiber reinforced polymer arch members. (Masters thesis, University of Maine, 2009).

Burgueno, R. (1999). System characterization and design of modular fiber reinforced polymer (FRP) short- and medium-span bridges. (Doctoral dissertation, University of California, San Diego, 1999) (UMI No. 9928617).

Clapp, J.D. and Davids, W.G. (2011). "Simplified Modeling to Assess Soil-Structure Interaction." AEWC Report No. 11-30.

Cox, B. N. and Dadkhah M. S. (1995). The macroscopic elasticity of 3D woven composites. *Journal of Composite Materials*, 29, 785-819.

Dagher, H.J., Bannon D.J., Davids, W.G., Lopez-Anido, R.A., Nagy, E., Goslin, K. (2012). "Bending behavior of concrete-filled tubular FRP arches for bridge structures." *Construction and Building Materials*, 37, 432-439.

Daniel, I. M. and Ishai, O. (2006). Engineering mechanics of composite materials, 2nd Edition. Oxford, NY.: Oxford University Press.

Davids, W.G., Walton, H.J., Clapp, J.D., Lopez-Anido, R., Goslin, K. and Dagher, H.J. (2012). "Response of concrete-filled tubular FRP arches to construction-induced loading." *Proceedings of the 2012 International Bridge Conference*, Pittsburgh, PA, June 2012.

Demkowicz, M. (2011). Environmental durability of hybrid braided polymer matrix composites for infrastructure applications. (Master's thesis, University of Maine, 2011).

Holtz, R.D., Kovacs, W.D. (1981) *An Introduction to Geotechnical Engineering*, Prentice Hall, Upper Saddle River, New Jersey.

Mander, J.B., Priestley, M. J.N., Park R., (1988). "Theoretical stress strain model for confined concrete" ASCE Journal of Structural Engineering 114, 1804-1826.

Walton, H.J., (2011). Response of FRP arches to concrete filling loads. (Masters thesis, University of Maine, 2011).